# Heat transfer and combustion simulation of a 7-element GOX/$GCH_4$ rocket combustor

**By N. Perakis, A. Sternin, C. Roth AND O. J. Haidn**

Chair of Turbomachinery and Flight Propulsion, Technische Universität München
Boltzmannstr. 15, 85748 Garching b. München

Within the framework of the SFB-TRR 40 Summer Program 2017 the simulation of the flow inside an experimental rocket thrust chamber was undertaken in the Chair of Turbomachinery and Flight Propulsion (LTF) of the TUM. The rocket combustor is operated with gaseous oxygen (GOX) and gaseous methane ($GCH_4$) and the tests were carried out at the experimental test bench of the LTF. The combustor's injector consists of seven individual coaxial injector elements, while the chamber and nozzle segments are water-cooled. The results presented in this work were obtained with 3D RANS simulations using an adiabatic Flamelet formulation for the chemistry modeling. In order to take advantage of the symmetry provided by the geometry and the RANS formulation, a 30° computational domain was chosen, corresponding to half injector in the outer injector row. The main focus was placed on examining the effect of the different turbulent models on the flame structure and on the resulting macroscopic values such as pressure and wall heat flux. The obtained numerical values were compared to experimental measurements delivering a good agreement in the heat flux profile at the combustion chamber wall and a slight underestimation of the pressure profile of approximately 2.5%. Greater discrepancies were observed in the heat flux of the nozzle segment, which are however largely attributed to the experimental setup. The azimuthal variation of the heat flux was also examined and interestingly the heat flux showcased a local minimum at the position directly above the injector element, which was found to be counterintuitive. By also simulating a 120° domain with identical results, the use of symmetrical boundary condition was excluded from the possible reasons of this phenomenon. A further investigation of this observed effect is planned in the future.

## 1. Introduction

A very important step in the process of designing and optimizing new components or subsystems for rocket propulsion devices is the numerical simulation of the flow and combustion in them. Implementing CFD tools in the design process significantly reduces the development time and cost and allows for greater flexibility. The main requirements that a successful CFD tool must fulfill in order to be suitable for rocket engine applications is providing an accurate description of the heat loads on the chamber wall, the combustion pressure, combustion efficiency as well as performance parameters such as the specific impulse.

The reliability of a numerical tool lies in accurately describing the physical and chemical processes taking place within the thrust chamber. This is done by a set of models (and the corresponding numerical methods to solve them), which must be validated for the wide range of operating conditions that can occur in different types of rocket engines

(e.g. attitude control thrusters, launcher propulsion). In order to make CFD attractive in the design process, the choice of the used models should be such that the computational time does not become prohibitive, while still capturing the physics of the underlying phenomena with sufficient accuracy.

A significant step during the development of numerical tools for combustion and turbulence modeling in rocket engines is the validation of the models. Within this framework the Chair of Turbomachinery and Flight Propulsion (LTF) at the Technical University of Munich (TUM) has tested several different configurations of rocket combustors and propellant combinations, building an experimental data base which can be used in the validation process. As part of the SFB/TRR 40 Summer Program 2017 a test case from this data base was defined. The experimental rocket combustor is operated with gaseous oxygen (GOX) and gaseous methane ($GCH_4$) and has a multi-element injector. A detailed description of the test campaign can be found in Silvestri et al. [1]. Section 2 gives a short summary of the relevant experimental data used in the simulations.

In the present paper the numerical results of the LTF group from the simulation of the seven-element chamber are presented. A 3D RANS approach is used and the combustion modeling is based on the adiabatic Flamelet approach. Section 3 deals with the numerical setup and models applied in the simulation, whereas the results are presented in Section 4. Finally Section 5 gives an overall conclusion and summary of the results and points out the potential areas of improvement.

## 2. Description of the test case

In the context of the national research program Transregio SFB-TR 40 on "Technological Foundation for the design of thermally and mechanically high loaded components of Future Space Transportation System", the examined multi-injector combustion chamber was designed for GOX and $GCH_4$ allowing high chamber pressures (up to 100 bar) and film cooling behavior examination. One of the key aspects of the project is to improve the knowledge on heat transfer processes and cooling methods in the combustion chamber, which is mandatory for the engine design. The attention is focused, in particular, on injector-injector and injector-wall interaction. In order to have a first characterization of the injectors′ behavior, the multi-element combustion chamber is tested at low combustion chamber pressures and for a wide range of mixture ratios [2].

The seven-element rocket combustion chamber has an inner diameter of 30 mm and a contraction ratio of 2.5 in order to achieve Mach numbers similar to the ones in most rocket engine applications. The combustion chamber, depicted in Fig. 1, consists of four cylindrical water cooled chamber segments, as well as a nozzle segment (individually cooled), adding up to a total length of 382 mm. For the current study, shear coaxial injector elements are integrated. The test configuration includes the GOX post being mounted flush with respect to the injection face.

For the present test case an operating point with mean combustion chamber pressure of 18.3 bar and mixture ratio of 2.65 was chosen. The experimental data made available for the numerical simulations included the mass flow rates of oxygen and methane, the wall temperature, pressure profile and integral heat flux values. A summary of the test data is given in Tab. 1. For the determination of the heat flux values in the four chamber segments (A-D) and the nozzle (N), a calorimetric method is applied. The average heat flux of each chamber segment is determined by the enthalpy difference of the coolant between inlet and outlet. This is obtained by precise temperature mea-

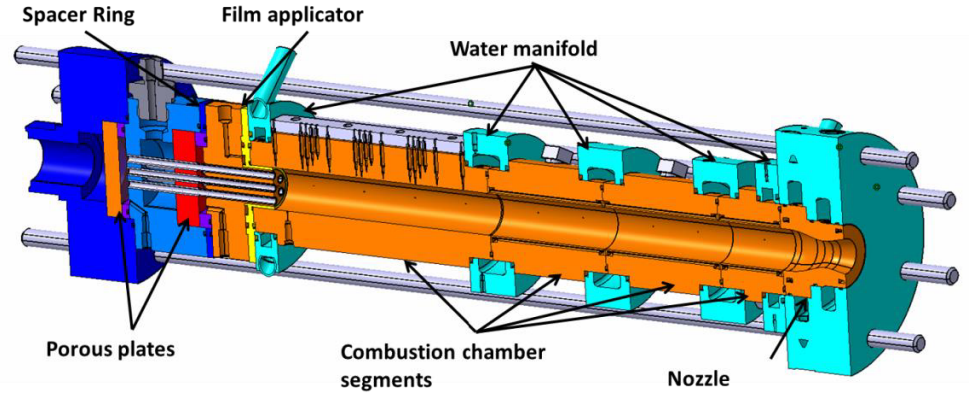


FIGURE 1. Sketch of the combustion chamber.

| | |
|---|---|
| Mean chamber pressure $P_c$ | $18.3\,\mathrm{bar}$ |
| Oxidizer to fuel ratio $O/F$ | $2.65$ |
| Oxidizer mass flow rate $\dot{m}_{ox}$ | $0.211\,\mathrm{kg/s}$ |
| Fuel mass flow rate $\dot{m}_{fu}$ | $0.080\,\mathrm{kg/s}$ |
| Average heat flux $\dot{q}_A$ | $3.40\,\mathrm{MW/m^2}$ |
| Average heat flux $\dot{q}_B$ | $6.47\,\mathrm{MW/m^2}$ |
| Average heat flux $\dot{q}_C$ | $6.72\,\mathrm{MW/m^2}$ |
| Average heat flux $\dot{q}_D$ | $5.37\,\mathrm{MW/m^2}$ |
| Average heat flux $\dot{q}_N$ | $13.18\,\mathrm{MW/m^2}$ |

TABLE 1. Summary of experimental data.

surements in the water manifolds between the test segments. The temperature values available are obtained at radial distances of 0.7-1.0 mm from the hot gas wall and were used as boundary conditions for the calculation, as will be elaborated on in Section 3.

## 3. Computational setup

The numerical computation for the simulation of the seven-element chamber was carried out using the pressure-based code Fluent, in which the 3D RANS equations were solved with the SIMPLE algorithm [3].

### 3.1. *Computational domain*

The computational domain considered in the RANS calculation consisted of a 30° segment of the thrust chamber, which included only half of the injectors in the outer row and corresponded to 1/12th of the whole chamber. In order to create a developed velocity profile at the injection plane, the injector tubes were also modeled as can be seen in Fig. 2. The final mesh consisted of approximately 3 million cells and was chosen after a mesh convergence study. In order to resolve the boundary layer appropriately and to facilitate a correct heat load prediction, the mesh in the vicinity of walls was refined as to satisfy the condition $y^+ \approx 1$.

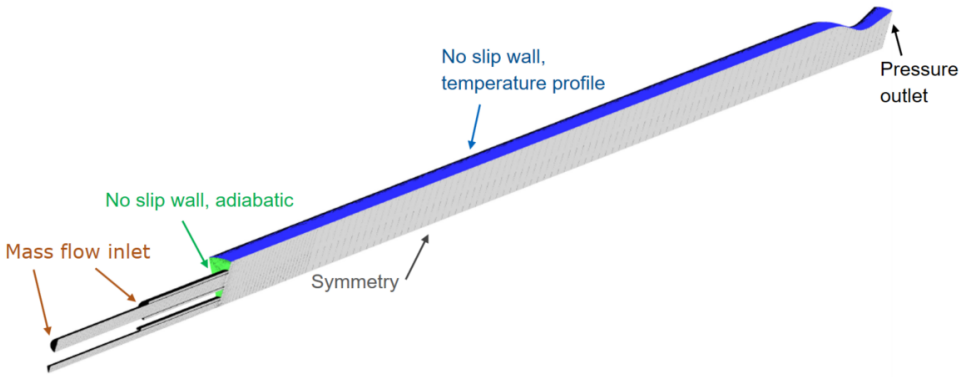


FIGURE 2. Computational domain and applied boundary conditions.

### 3.2. *Boundary conditions*

A schematic representation of the applied boundary conditions can be seen in Fig. 2. The oxygen and methane inlets of the coaxial injector were defined as mass flow inlets by prescribing the appropriate values from the experiments. For the outlet a pressure boundary condition was applied. The planes corresponding to 0 and 30° were defined as symmetry boundary conditions. This was chosen to reduce the computational time of the simulation and to take advantage of the RANS formulation which gives only the mean flow values. A further justification of this choice for the boundary condition is given in Section 4.4. At the chamber wall, a prescribed temperature profile was defined. This profile was obtained by the experimental values. Since the temperature measurements directly at the hot gas wall were not available, the ones at 0.7 mm and 1.0 mm were chosen instead. Although they underestimate the temperature directly at the wall, it has been found in previous studies that the effect on the wall heat flux is minimal and can be neglected. Since no temperature data were known at the nozzle, the last temperature value from the combustion chamber was defined at the nozzle wall. The resulting temperature profile at the wall is shown in Fig. 4 . All remaining walls were defined as adiabatic thermal boundaries and were given a no-slip condition. A close-up view of the mesh at the injector and faceplate is shown in Fig. 3. The green cells represent the faceplate wall, the black ones the post-tip between oxygen and fuel and the red and blue cells the $CH_4$ and $O_2$ inlets respectively.

### 3.3. *Numerical models*

As already mentioned, the chemistry modeling took place by using the Flamelet approach. This model significantly reduces the computational resources required for combustion simulations by reducing the number of transport equations. This is done by replacing the transport equations for the chemical species by only two equations: one for the mean mixture fraction $\tilde{Z}$ and one for its variance $\tilde{Z''^2}$. The variance of the mixture fraction is included in order to account for the interaction between the chemistry and the turbulence. A third variable which is calculated by the model (but with an algebraic equation instead of a transport one [3]) is the scalar dissipation rate $\tilde{\chi}$. This represents the dissipative term in the equation for the mixture fraction variance and is a measure for the deviation of the flow from the equilibrium. A value of $\tilde{\chi}$ equal to zero would imply a perfect mixing and a low strain rate in the flow and would correspond to

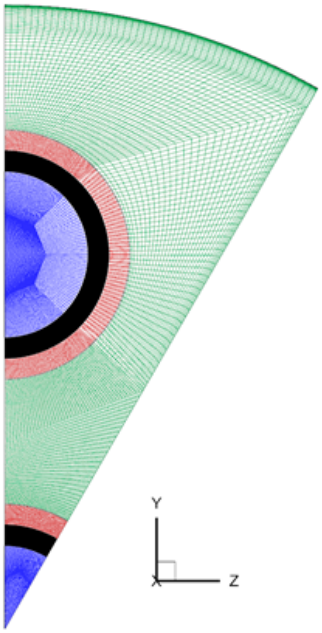


FIGURE 3. Mesh at injector elements and faceplate.

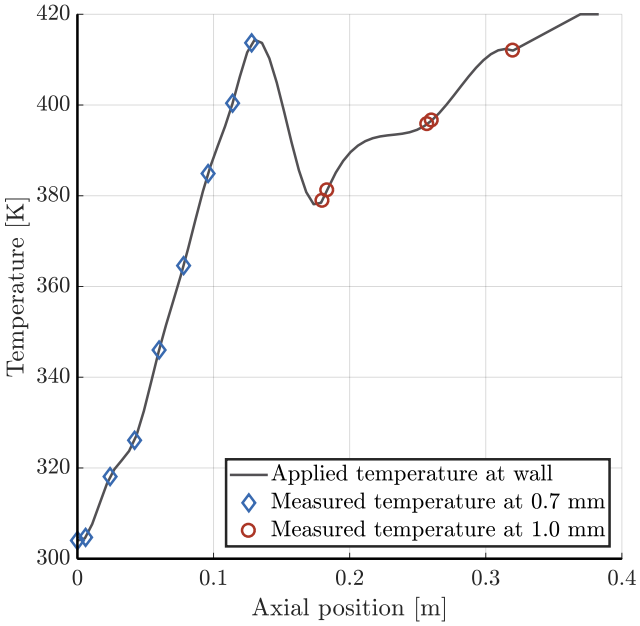


FIGURE 4. Temperature at thrust chamber wall.

chemical equilibrium. For much higher values of this quantity, the extinction limit of flame is reached [4].

The properties of the mixture such as the mixture fractions of the individual species as well as the temperature are pre-tabulated as a function of the laminar variables $Z$ and $\chi$. This is done by solving the Flamelet equations in a pre-processing step. They consist of a transport equation for the temperature $T$ and for the species mass fractions $Y_i$ as shown in Eqs. 3.1 and 3.2 [5], [3]:

$$\rho\frac{\partial T}{\partial t} = \frac{1}{2}\rho\chi\frac{\partial^2 T}{\partial Z^2} - \frac{1}{c_p}\sum_i H_i\dot{\omega}_i + \frac{1}{2c_p}\rho\chi\left[\frac{\partial c_p}{\partial Z} + \sum_i c_{p,i}\frac{\partial Y_i}{\partial Z}\right]\frac{\partial T}{\partial Z} \tag{3.1}$$

$$\rho\frac{\partial Y_i}{\partial t} = \frac{1}{2}\rho\chi\frac{\partial^2 Y_i}{\partial Z^2} + \dot{\omega}_i \tag{3.2}$$

In this context $\dot{\omega}_i$ represents the species reaction rate and $H_i$ the specific enthalpy of each species.

The Flamelet equations are solved for different values of the scalar dissipation, leading to a laminar table $T, Y_i = f(Z, \chi)$. In order to account for the turbulence-chemistry interaction (TCI), a further step is undertaken during pre-processing. A statistical treatment of turbulence is included by performing an integration using a Presumed Probability Density Function (PPDF). For each value of the mean mixture fraction, mixture fraction variance and mean scalar dissipation, the PPDF is calculated and an integration takes place according to Eqs. 3.3 and 3.4.

$$\tilde{Y}_i\left(\tilde{Z}, \tilde{Z''^2}, \tilde{\chi}\right) = \int_0^\infty \int_0^1 Y_i(Z,\chi)\cdot P(Z,\chi)\mathrm{d}Z\mathrm{d}\chi \tag{3.3}$$

$$\tilde{T}\left(\tilde{Z}, \tilde{Z''^2}, \tilde{\chi}\right) = \int_0^\infty \int_0^1 T(Z,\chi) \cdot P(Z,\chi) \mathrm{d}Z \mathrm{d}\chi \tag{3.4}$$

The resulting mean species mass fractions and mean temperature are hence tabulated as a function of the three flow variables $\tilde{Z}, \tilde{Z''^2}, \tilde{\chi}$. The PPDF chosen in this work is a decoupled PDF, i.e $P(Z,\chi) = P(Z) \cdot P(\chi)$, with beta PDF for the mixture fraction and a Dirac function for the scalar dissipation.

During the CFD computation, the transport equations for the mean mixture fraction and its variance are solved as well as the scalar dissipation is computed algebraically for each cell. With this information the species mass fractions are interpolated from the pre-computed Flamelet table. With the specific enthalpy of the cell, the temperature can be obtained. In the present work, an adiabatic (or else "frozen") Flamelet approach was used. This means that the mass fractions are not tabulated as a function of the enthalpy. This simplification suppresses further reactions which could take place in the presence of a lower enthalpy - for example recombinations close to the wall. Although this effect is considered to be significant and is probably not negligible, in the present work the model has been simplified and the enthalpy is only used to correct the resulting temperature (and hence density as well).

The reaction mechanism used for the solution of the Flamelets is the one by Slavinskaya et al. [6] and consists of 21 species and 97 reactions, whereas the thermodynamic properties were calculated using NASA polynomials. For the molecular transport (viscosity and thermal conductivity) the kinetic theory was utilized, leading to species- and temperature-dependent properties [7]. Different turbulence models were compared as seen in Sec. 4 but the standard $k-\epsilon$ model showed the most promising results, using a two-layer model for the wall treatment.

## 4. Results

In this section the results of the CFD calculations will be presented and compared with the experimental values. In the first approach, the standard $k-\epsilon$ combined with the two-layer model at the wall was implemented and compared to the $k-\omega$ SST with low-Reynolds correction. For both approaches, the closure of the tubulent flux terms was done with a turbulent Schmidt number $Sc_t = 0.6$ and a turbulent Prandtl number $Pr_t = 0.9$.

In Figs. 5 and 6 the temperature field inside the thrust chamber is plotted. Although a 30° domain was simulated, a larger domain (150°) is shown in the plots for a more intuitive visual representation. In the same plot, the line corresponding to stoichiometric composition ($Z_{st} \approx 0.2$) in the case of $CH_4/O_2$ combustion is indicated. This is included to give an insight into the shape of the flame and consequently its length.

### 4.1. *Effect of turbulence model on mixing and combustion*

By examining the two distributions, it is evident that the $k-\epsilon$ models tends to better capture the mixing within the combustion chamber. In the SST model, the temperature stratification remains prominent even in axial positions close to the nozzle. The temperature demonstrates namely a "wavy" pattern especially close to the wall, which is an indication for inefficient mixing of the individual flames. In the $k-\epsilon$ however, this temperature stratification is restricted to the first two thirds of the engine and a more homogeneous field is present further downstream. The effect of the less efficient mixing

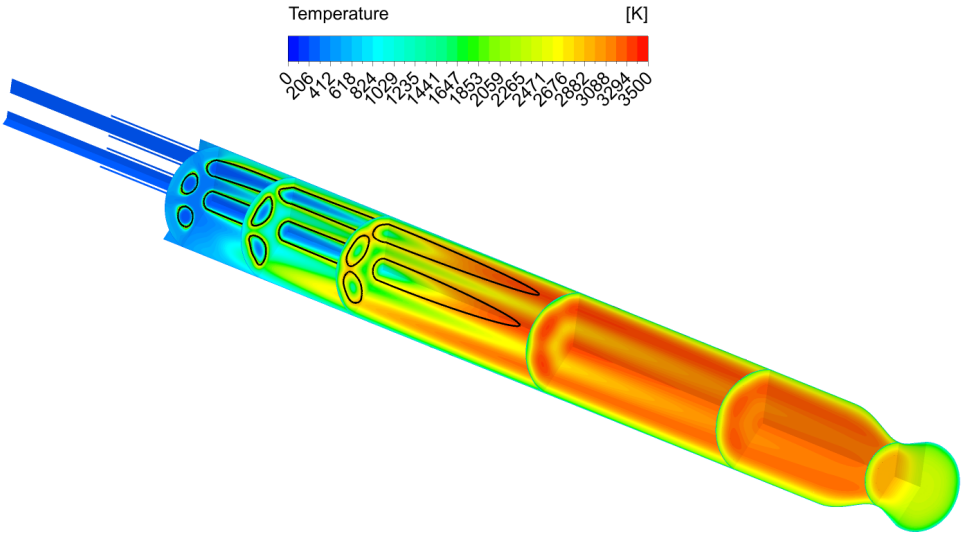


FIGURE 5. Temperature field in the thrust chamber using the standard $k-\epsilon$ model (the black line corresponds to the stoichiometric mixture fraction).

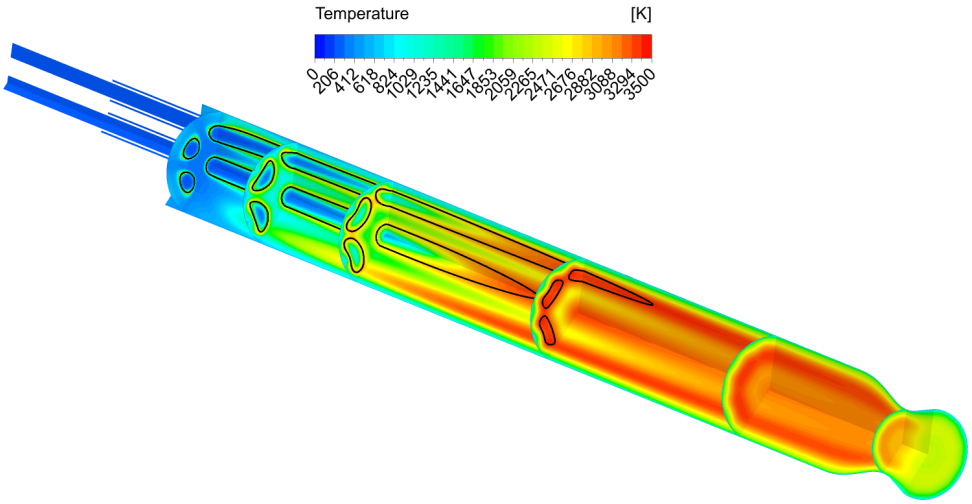


FIGURE 6. Temperature field in the thrust chamber using the $k-\omega$ SST model (the black line corresponds to the stoichiometric mixture fraction).

is also evident by the length of the individual flames. In the $k-\epsilon$ results the outer and inner flames are almost equally long and extend up until the middle of the chamber. The SST on the other hand produces a sufficiently longer flame length, more dominantly in the outer flame implying a smaller flame-flame and flame-wall interaction.

The effect was attributed to a lower production in the turbulent viscosity of the SST model. Figures 7 and 8 demonstrate that the turbulent viscosity resulting from the $k-\epsilon$ calculation has a higher value throughout the whole combustion chamber, leading to a higher "dissipation" and hence a more uniform temperature field. The effect is mainly prominent in the area of the individual flame jets and in the core flow. The $k-\epsilon$ calculation

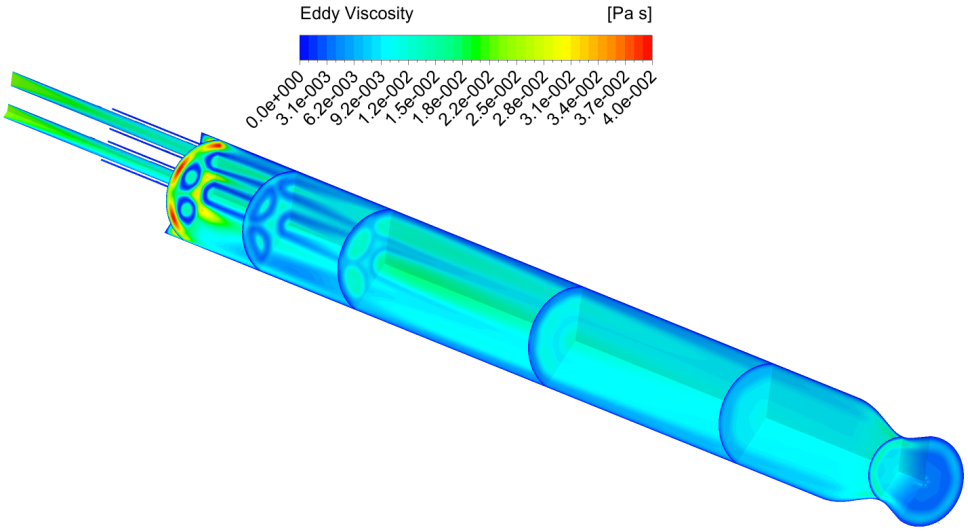


FIGURE 7. Turbulent viscosity field in the thrust chamber using the standard $k - \epsilon$ model.

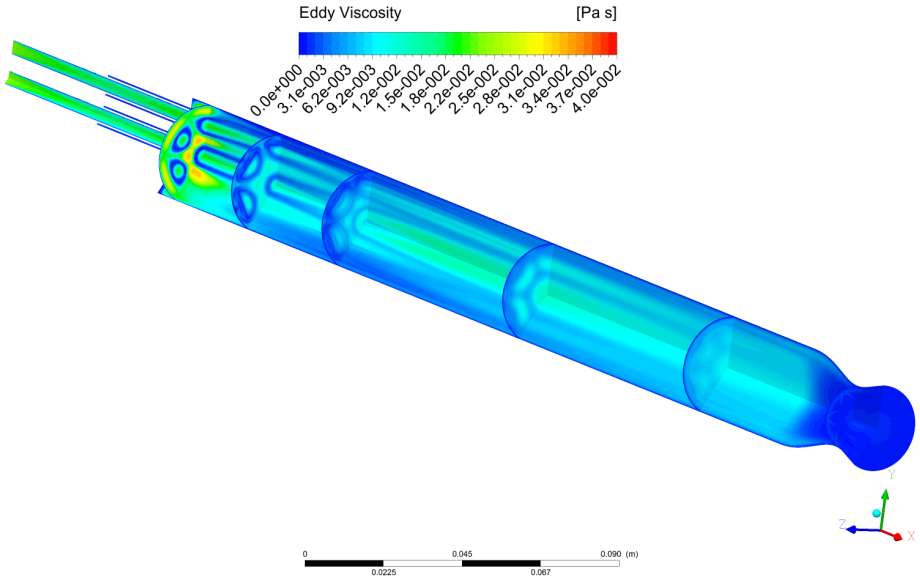


FIGURE 8. Turbulent viscosity field in the thrust chamber using the $k - \omega$ SST model.

was performed with the use of a limiter for the turbulent kinetic energy according to Menter et al. [8]. Calculations without the limiter resulted in the presence of a large area with very high turbulent viscosity at the nozzle. This effect was restrained close to the axis of the nozzle and was dampened out closer to the wall. Although the production limiter led to the disappearance of this hot-spot, making the $\mu_t$-field more "intuitive", no measurable changes in the macroscopic values such as pressure or heat flux in the nozzle were observed.

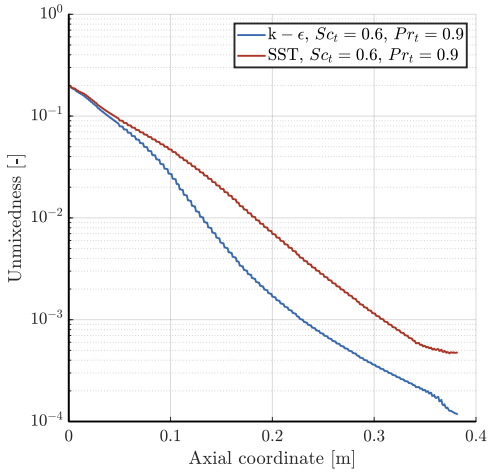


FIGURE 9. Unmixedness along the axial position.

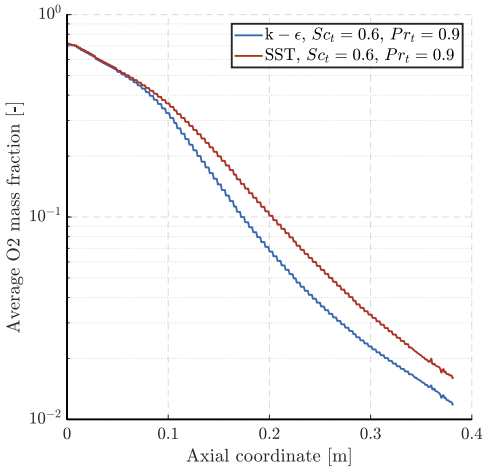


FIGURE 10. Average $O_2$ mass fraction along the axial position.

A more quantitative examination of the inefficient mixing in the chamber is given by evaluating the unmixedness and the average $O_2$ mass fraction in the thrust chamber. The unmixedness is a dimensionless number which describes the degree of mixing in the chamber. For an ideal mixture, it reaches the value 0, whereas for totally unmixed compounds, it is equal to 1. Its formula is given by Eq. 4.1.

$$U = \frac{\langle Z"^2 \rangle}{\langle Z \rangle (1 - \langle Z \rangle)} \tag{4.1}$$

$\langle Z \rangle$ stands for the average mixture fraction along all the nodes of a cross sectional plane and $\langle Z"^2 \rangle$ for the variance of the mixture fraction values on these points. The unmixedness should approach zero towards the exit plane of the nozzle, due to increasingly better mixing of the gas. The $k - \epsilon$ shows an unmixedness value approximately 5 times larger at the exhaust plane and a generally larger value along the whole domain of the chamber, which confirms the fact that the mixing is calculated more effectively.

A further quantity which acts as a measure for the degree of mixing and the completion of combustion is the concentration of oxygen in the combustion chamber. In order to achieve the maximum yield from the reaction of the propellants and hence the highest possible energy release, the amount of unburnt oxygen leaving the chamber should be held at a minimum. Equilibrium calculations using Cantera [9] showed that a mass fraction of approximately 0.2-0.4% $O_2$ is expected at equilibrium. Both turbulence models seem to over-predict the oxygen at the outlet, thereby underpredicting the mixing and the energy release in the chamber. The $k - \epsilon$ and SST models show that approximately 1.40% and 1.75% $O_2$ remain unburnt respectively. Therefore, although the $k - \epsilon$ produces better results that the SST, it still fails to capture the mixing and energy release correctly when combined with the Flamelet model.

### 4.2. *Comparison with experimental results*

An additional indicator for the incompleteness of the combustion is the lower chamber pressure, as can be seen in Fig. 11. Both turbulence models underestimate the pressure in the chamber by approximately 0.4 bar. The pressure profile however seems to be very

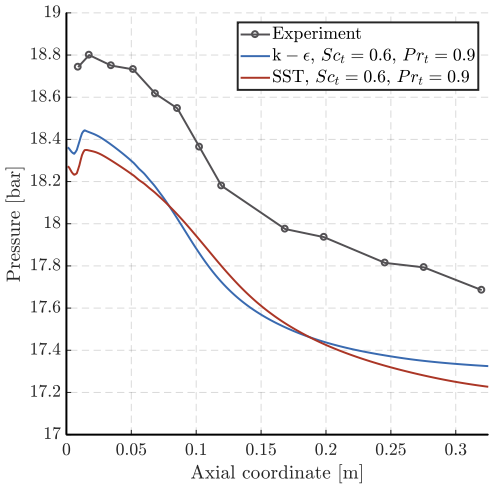


FIGURE 11. Average pressure along the axial position of the combustion chamber.

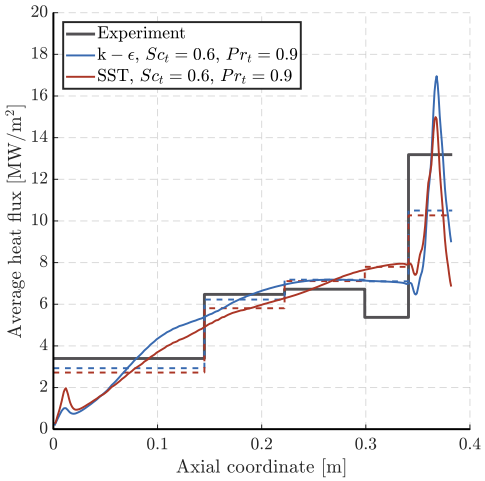


FIGURE 12. Average wall heat flux along the axial position.

similar with the experimental one, implying similar acceleration profiles for the hot gas in the simulation and the experiment. The SST pressure profile seems to be slightly steeper close to exit of the combustion chamber and the start of the nozzle, meaning that the energy release and the acceleration of the gas is still ongoing.

This is also the case with the heat flux, which keeps increasing even in the last chamber segment for the SST case, as can be seen in Fig. 12, where the local average heat flux (solid line) as well as the integrated heat flux for each segment (dashed line) are illustrated. Both models deliver a good match with the experimental data in the first three segments of the chamber. The $k - \epsilon$ results show an increase of the heat flux over the first two segments and a flatter profile for the last two, indicating that the heat release has ended. In the segment D however, a drop in the heat flux is measured in the experiments, whereas the simulation predicts either a flat profile ($k - \epsilon$) or an increase of the heat loss to the wall (SST). This along with the very high heat flux measured in the nozzle (compared to the CFD), are the main discrepancies between simulation and experiment. In fact, the nozzle heat flux has an error of approximately 25%. Further CFD tests were carried out by decreasing the wall temperature boundary condition since the actual value of the temperature is unknown. Even unrealistic values of 300 K at the wall were still unable to capture such a high increase in the nozzle heat flux. Changing the turublence close numbers ($Pr_t$ and $Sc_t$) did not introduce any improvement in this aspect.

A further investigation of the results and discussion with the publishers of the experimental results attributed the discrepancies in the segments D and N to the experimental setup. Specifically, the nozzle has a separate cooling cycle and for this test case a very large water mass flow rate was chosen, in order to avoid any mechanical damage of the copper. The overly large coolant flow led to lower temperatures in the material and therefore to an axial heat flow from the segment D into the nozzle segment. Energy which was originally applied to the wall of the fourth segment diffused axially towards the lower temperature domain of the nozzle segment. The consequence was that the water in the nozzle would pick up a higher energy whereas the water in the last segment

would not be heated as much as expected, thereby producing a significant drop in the heat flux of the third segment and a high increase in the nozzle.

### 4.3. *Investigation of the experimental heat flux in the nozzle*

This effect was also validated using an in-house engineering thermal code at the LTF called Thermtest [10]. Thermtest allows the simulation of steady as well as transient thermal behavior of cooled or uncooled structures over a wide scope of chamber materials and cooling fluids. While the heat conduction inside the chamber material is solved by a 3D finite difference method, the convective heat transfer from the hot gas side to the inner wall as well as for the coolant is modeled using empirical Nusselt correlations [11].

The present test case was also simulated using Thermtest in order to understand the heat exchange between the segments better and the results are shown in Fig. 13. The solid blue line represents the wall heat flux predicted by a modified Cinjarev correlation [12], whereas the dashed line the integrated values for each segment directly at the wall. The solid red line represents the heat flux resulting from the enthalpy difference of the incoming and outgoing water at each segment. This is similar to the measurement performed during the experiment.

The assumption of the experimental technique is that the wall heat flux and the one resulting from the enthalpy difference should be identical if the whole heat load is captured by the water. Due to the high mass flow at the nozzle segment however, the water enthalpy in segment D substantially decreases, whereas the one in the nozzle shows an increase. Hence the assumption of the axial heat flux altering the experimental data was confirmed and no further comparison with the CFD nozzle result was carried out. A correct representation would require a thermally coupled simulation of the hot flow and the coolant flow, which was however not performed due to the high computational time required.

### 4.4. *Azimuthal heat flux profile*

A very interesting observation occurred when investigating the variation of the heat flux along the chamber angle. The azimuthal profile of the heat flux at the wall is shown in Fig. 14. Here 0° corresponds to the position directly above the injector and -30°, 30° to the symmetry planes, while 0 mm refers to the faceplate and 300 mm is a plane approximately 40 mm before the end of the combustion chamber and the beginning of the nozzle. As expected, the SST model produces a much larger variation of the heat flux value along the perimeter, since it has a higher temperature stratification even at positions close to the nozzle. The $k-\epsilon$ on the other hand demonstrates a flat heat flux profile for positions after 200 mm, in agreement with the temperature field (Fig. 5), which becomes homogeneous.

An unexpected effect is that for both models, the heat flux has a local minimum at the position directly above the injector (0°) and its maximum at approximately 15°. This effect starts after about 50 mm downstream of the injector and continues for the rest of the chamber. In order to better understand the origin of this phenomenon, the temperature was plotted at the wall as seen in Fig. 15. At the wall position, the mixture fraction variance and the scalar dissipation tend to zero and hence the temperature becomes a function of the mixture fraction solely (and the enthalpy, whose effect however is negligible in the adiabatic Flamelet formulation). For that reason the mixture fraction is also plotted in Fig. 15. This is done only for the $k-\epsilon$ model, since it is the one producing the more physical results.

As expected, the temperature has a maximum directly at the positions where the

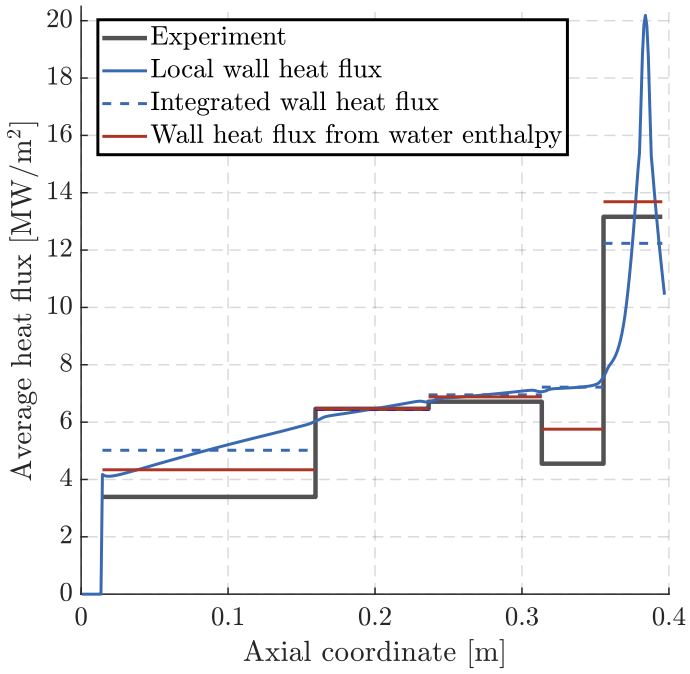


FIGURE 13. Heat flux profiles resulting from the Thermtest calculation.

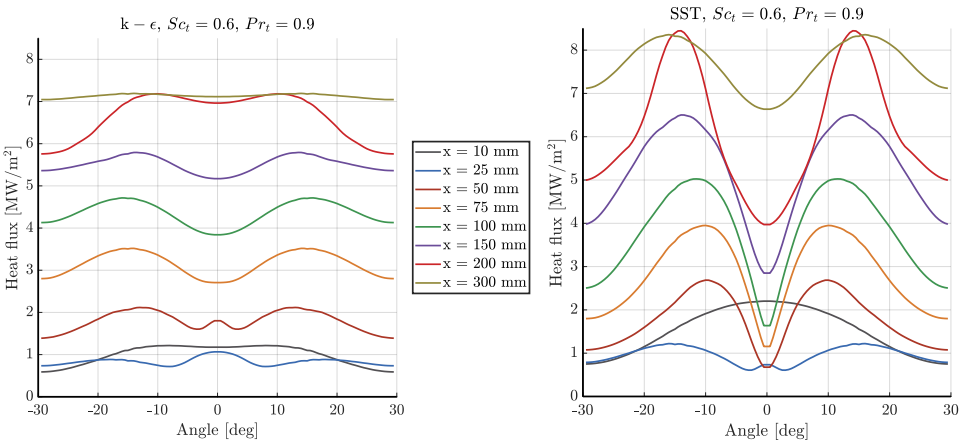


FIGURE 14. Heat flux variation along the chamber angle for different axial positions.

heat flux is also maximal and a minimum at 0°. This is a result of the mixture fraction profiles at the wall: after the stoichiometric mixture fraction $Z_{st} \approx 0.2$, the temperature decreases with increasing mixture fraction and hence, the local maximum of the heat flux corresponds to a lower value of $Z$, i.e. a leaner composition and vice versa. This is validated in the right sub-figure of Fig. 15. For positions closer to the injector, a recirculation zone is created which leads to a maximum in heat flux right above the injector. Further downstream pockets of fuel-rich mixture are created directly at 0° which lead to a decrease in temperature and heat flux.

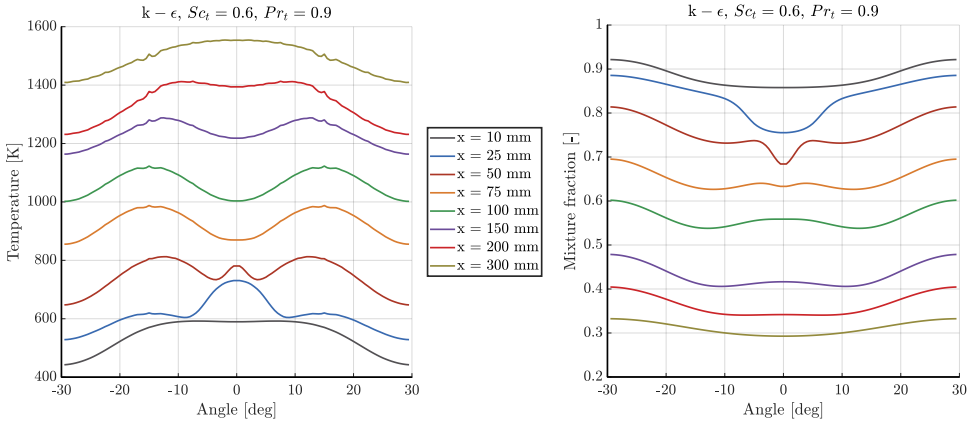


FIGURE 15. Azimuthal variation of temperature and mixture fraction at the wall for the $k - \epsilon$ model.

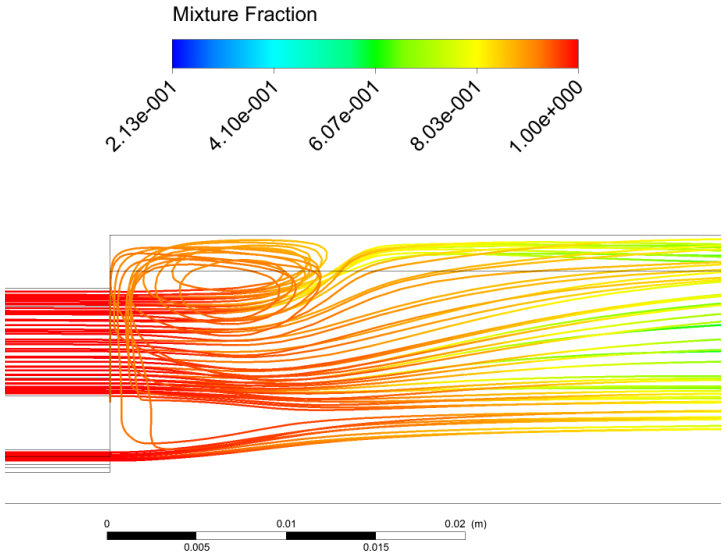


FIGURE 16. Streamlines coming from the fuel inlet coloured by mixture fraction.

The streamlines in Fig. 16 and Fig. 17 verify that. In Fig. 16, the length of the recirculation zone is visible, amount to approximately 10 mm, whereas in Fig. 17 the cause of the higher mixture fraction at 0° is illustrated. It can be observed that after the location of the recirculation zone, a twist in the flow takes place. Specifically, due to the interaction of the injector jet with the symmetry boundary condition (i.e. with the neighboring injector), areas with high mixture fraction are pushed towards the middle. This leads to an accumulation of the fuel rich zones above the injector, leading to a lower temperature.

In order to make sure that the effect is not caused by the symmetry boundary condition applied between the injectors, it was decided to extend the computational domain to include 120° of the rocket combustor. This would have the effect of modeling two full injectors at the outer row (instead of half) as well as one direct interaction between

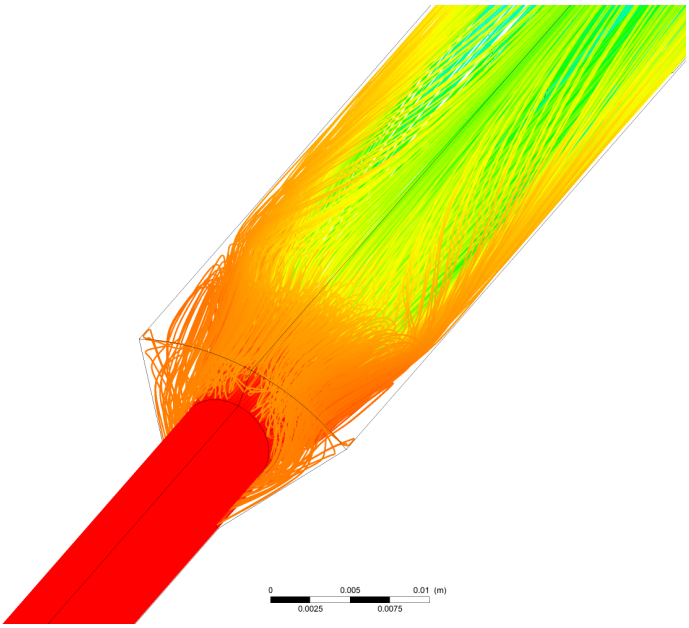


FIGURE 17. Streamlines coming from the fuel inlet coloured by mixture fraction.

the injectors and one throught the symmetry boundary condition. In order to keep the computational mesh intact, the original mesh was simply reflected onto the symmetry plane as to maintain the same resolution.

The results demonstrated an identical heat flux profile as the 30° calculation, indicating that the symmetry boundary condition is not the source of the local minimum. As can be seen in Fig. 18, the same change in the flow direction due to the interaction between the injectors is also visible (note the difference in color scaling compared to Fig. 17). This effect is therefore a result of the turbulence model, the chemistry model and the flow interaction between the injectors. Further studies with other chemical models should be carried out to examine if this is only produced due to the use of the Flamelet approach. Further measurement data such as an azimuthal heat flux profile would also be beneficial in order to allow a comparison with the CFD.

## 5. Conclusions

Within the framework of the SFB-TRR 40 Summer Program 2017 a 3D RANS simulation of a seven-element rocket thrust chamber operated at the Chair of Turbomachinery and Flight Propulsion of the TUM was carried out. For the simulation, an adiabatic Flamelet approach was implemented using a skeletal chemical mechanism.

Two different turbulence models were compared to each other and specifically the $k-\epsilon$ with a two-layer model was compared to the $k-\omega$ SST. It was found that the $k-\epsilon$ produced more physical results in the combustion chamber, since it facilitated mixing, whereas the SST produced a very large temperature stratification of the temperature, which propagated further downstram till the nozzle. This was attributed to a much lower turbulent viscosity in the main flow. However even the $k-\epsilon$ was found to have inefficient mixing and a lower heat release than theoretically expected. This was evident due to a

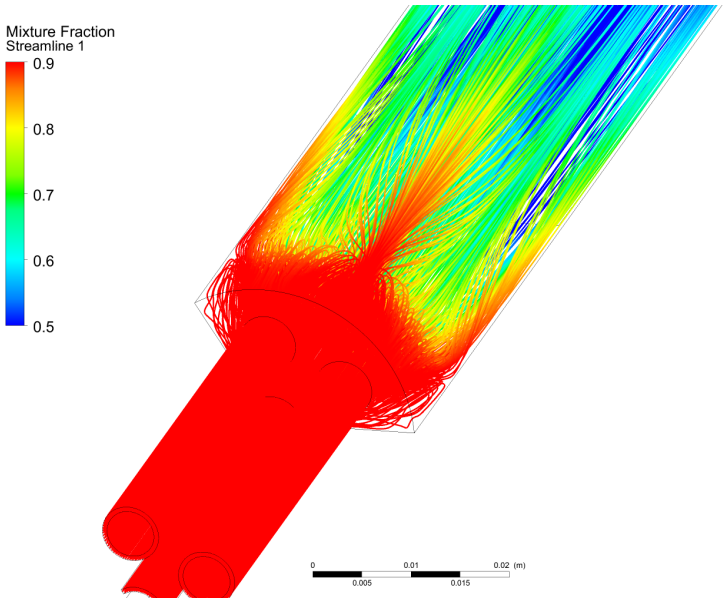


FIGURE 18. Streamlines coloured by mixture fraction for the 120° domain.

high unmixedness at the exit, a high mass fraction of unburnt oxygen and a chamber pressure lower than the experimental one by 2.5%.

Apart from the pressure, comparison with the experimental heat flux took place. The CFD simulation was able to reproduce the heat flux values in the first three segments of the combustion chamber, but produced a high discrepancy in the last segment and in the nozzle. With a separate thermal analysis it was found that the experimental setup led to an unrealistically high measured heat flux in the nozzle due to an overestimated water coolant mass flow rate. Hence, no further comparison was made with the heat flux results at the nozzle.

Finally, it was observed that the heat flux coming from the CFD had a local minimum directly above the injector position (0°) as opposed to a maximum. This was attributed to the interaction between the individual jets leading to low temperature gas staying trapped diretly above the injector position. A further simulation with a 120° domain confirmed that this effect was not a product of the symmetry boundary conditions.

Further examination of this test case is planned for the future. A coupled simulation with a thermal solver will be carried out in order to better understand the processes taking place in the nozzle. For an improved modeling of the heat transfer with the wall, a non-adiabatic Flamelet model will be applied in the future, which will include heat loss effects in the concentration of the species via recombination. Further evaluation of the test results is also scheduled: by developing an inverse heat transfer method, the azimuthal distribution of the heat flux could be reconstructed based on the temperature measurements at the wall. This would allow for a verification or disproof of the heat flux profile along the chamber perimeter. Simulations with different chemistry models (such as Finite Rate Chemsitry or Eddy Dissipation Concept) will also be carried out to see if the behaviour of the jet interaction remains.

## Acknowledgments

Financial support has been provided by the German Research Foundation (Deutsche Forschungsgemeinschaft – DFG) in the framework of the Sonderforschungsbereich Transregio 40.

## References

[1] SILVESTRI, S., KIRCHBERGER, C., SCHLIEBEN, G., CELANO, M.P. AND HAIDN, O.J. (2017). Experimental and numerical investigation of a multi-injector gox-gch4 combustion chamber. In: *31st International Symposium on Space Technology and Science (ISTS)*. Japan.

[2] SILVESTRI, S., CELANO, M.P., SCHLIEBEN, G. AND HAIDN, O.J. (2016). Characterization of a multi-injector gox-gch4 combustion chamber. In: *Joint Propulsion Conference, JPC2016*.

[3] FLUENT, A. (2011). Ansys fluent theory guide. *ANSYS Inc., USA*, **15317**, 724–746.

[4] PETERS, N. (1984). Laminar diffusion flamelet models in non-premixed turbulent combustion. *Progress in energy and combustion science*, **10**(3), 319–339.

[5] PITSCH, H., BARTHS, H. AND PETERS, N. (1996). *Three-dimensional modeling of NOx and soot formation in DI-diesel engines using detailed chemistry based on the interactive flamelet approach*. Tech. rep., SAE Technical Paper.

[6] SLAVINSKAYA, N., ABBASI, M., STARCKE, J.H., MIRZAYEVA, A. AND HAIDN, O.J. (2016). Skeletal mechanism of the methane oxidation for space propulsion applications. In: *52nd AIAA/SAE/ASEE Joint Propulsion Conference*. 4781.

[7] PITSCH, H. (1993). Entwicklung eines programmpaketes zur berechnung eindimensionaler flammen am beispiel einer gegenstromdiffusionsflamme. In: *Master's thesis*. Technical University of Aachen Aachen Germany.

[8] MENTER, F.R. ET AL. (1994). Two-equation eddy-viscosity turbulence models for engineering applications. *AIAA journal*, **32**(8), 1598–1605.

[9] GOODWIN, D.G., MOFFAT, H.K. AND SPETH, R.L. (2017). Cantera: An object-oriented software toolkit for chemical kinetics, thermodynamics, and transport processes. `http://www.cantera.org`. Version 2.3.0.

[10] KIRCHBERGER, C., SCHLIEBEN, G. AND HAIDN, O. (2012). Assessment of analytical models for film cooling in a hydrocarbon/gox rocket combustion chamber. In: *48th AIAA/ASME/SAE/ASEE Joint Propulsion Conference & Exhibit*. 3909.

[11] KIRCHBERGER, C., WAGNER, R., KAU, H.P., SOLLER, S., MARTIN, P., BOUCHEZ, M. AND BONZOM, C. (2008). Prediction and analysis of heat transfer in small rocket chambers. In: *46th AIAA Aerospace Sciences meeting and Exhibit, AIAA-2008-1260, Reno (NV), USA*. 07–11.

[12] SCHMIDT, G. (1999). Technik der flüssigkeits-raketentriebwerke. *Daimler-Chrysler Aerospace, Munich*.